OPEN ACCESS
IOP Publishing
Journal of Physics B: Atomic, Molecular and Optical Physics
J. Phys. B: At. Mol. Opt. Phys. **53** (2020) 124002 (7pp)
https://doi.org/10.1088/1361-6455/ab7c3f

# Attosecond transient absorption of a continuum threshold

**Paul Birk[1,3], Veit Stooß[1], Maximilian Hartmann[1], Gergana D Borisova[1], Alexander Blättermann[1], Tobias Heldt[1], Klaus Bartschat[2], Christian Ott[1] and Thomas Pfeifer[1,3]**

[1] Max-Planck-Institute for Nuclear Physics, Saupfercheckweg 1, D-69117 Heidelberg, EU, Germany
[2] Department of Physics and Astronomy, Drake University, Des Moines, IA 50311, United States of America

E-mail: birk@mpi-hd.mpg.de and tpfeifer@mpi-hd.mpg.de

Received 6 December 2019, revised 5 February 2020
Accepted for publication 3 March 2020
Published 27 May 2020

**Abstract**

The laser-field-modified dipole response of the first ionization threshold of helium is studied by means of attosecond transient absorption spectroscopy. We resolve light-induced time-dependent structures in the photoabsorption spectrum both below and above the ionization threshold. By comparing the measured results to a quantum-dynamical model, we isolate the contributions of the unbound electron to these structures. They originate from light-induced couplings of near-threshold bound and continuum states and light-induced energy shifts of the free electron. The ponderomotive energy, at low laser intensities, is identified as a good approximation for the perturbed continuum response.

Keywords: attosecond, ionization threshold, time-resolved spectroscopy

(Some figures may appear in colour only in the online journal)

With the advent of high-order harmonic generation, it became possible to generate extreme ultraviolet (XUV) pulses on the attosecond time scale, which paved the way for direct time-resolved measurements on the natural time scale of electronic excitations. A number of experiments using these pulses have since been developed for the study of light–matter interaction of gaseous atomic, molecular, and solid-state systems [1–7]. In these experiments, one typically records either the spectrum of photoionized fragments, i.e. the photoelectrons and/or the -ions, or the photoabsorption spectrum of a target under investigation.

In the first case, the target is always ionized, meaning at least one electron is excited into the continuum. In typical experiments the ionization is achieved by either multiphoton and/or multicolor ionization or single-photon ionization in the presence of a second time-delayed (strong) laser pulse. By measuring the photoelectron/-ion yield or spectra in an interferometric and time-resolved manner one is sensitive to phases between different ionization pathways or streaking traces [8]. This phase sensitivity gives access to and control of e.g. phases of resonant transitions [9–11], temporal structure of the laser pulses [12] or ionization delays on the attosecond time scale [13, 14].

The ionization delays are governed by the interaction of the free electron with the residual electrons and the ionic core during the ionization process. Slow electrons, i.e. photoelectrons excited with photon energies closely above the ionization threshold, remain longer in the vicinity of the parent ion and obtain larger phase shifts [15]. Furthermore, since the impact of the Coulomb potential is not negligible for slow electrons, the strong-field approximation breaks down [16]. All these circumstances motivate direct measurements of light-induced time-dependent structures on slow photoelectrons that are energetically close to an ionization threshold [16–22].

Recording the XUV photoabsorption spectrum in the presence of the second laser field gives access to light-induced

[3] Authors to whom any correspondence should be addressed.

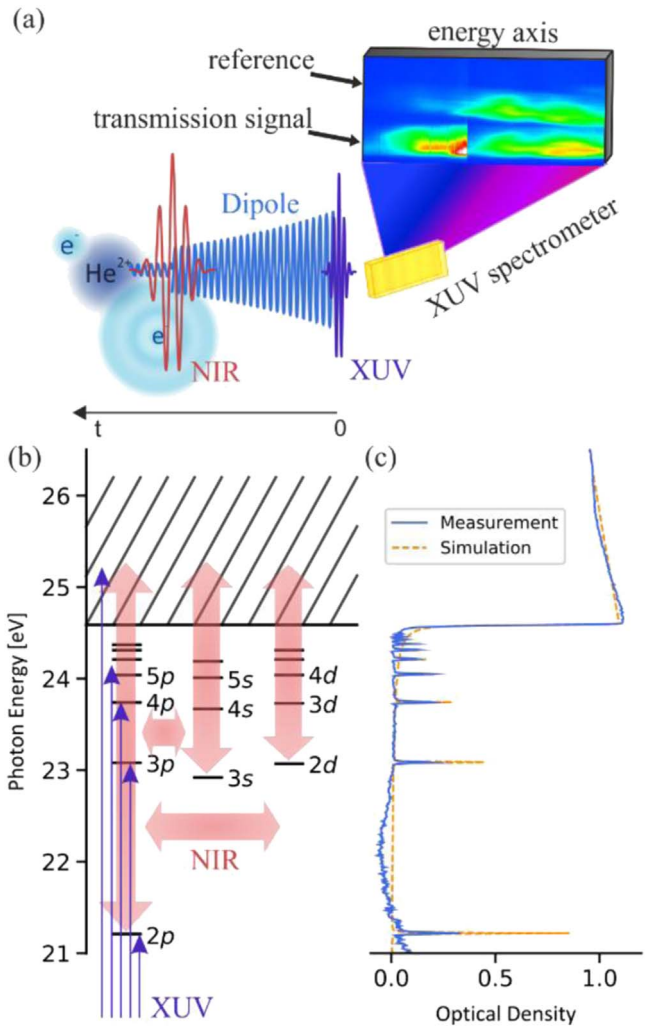


**Figure 1.** (a) Time-domain sketch of the underlying physics of the light-induced modification of an absorption spectrum. Real time increases from right to left. The XUV-induced freely decaying dipole moment (blue) interferes with the XUV light (violet) in time, which leads to the absorption spectrum that is recorded by the spectrometer. The dipole moment is caused by the coupling between ground and excited or continuum states, illustrated by the displaced electron cloud. An NIR pulse (red) modifies the dipole moment at a certain time after XUV excitation, which leads to changes of the XUV absorption spectrum. (b) Energy-level diagram of helium. The XUV pulse excites or ionizes the helium atom (violet thin arrows). The NIR pulse induces couplings between the states and also with the continuum (red big arrows). (c) Lineouts of the measured (solid, blue) and the simulated (dashed, orange) XUV absorbance. The energy axis is shared with subfigure (b).

dynamics on electronic bound states of a system. State-specific transitions between bound states can be resolved far below or also close to an ionization threshold. Typical modifications in the XUV absorption spectra are light-induced states, oscillations of the absorption line strength, or hyperbolic structures with respect to the time delay of an intense optical laser pulse [23–27].

These spectral modifications can be understood as laser-induced changes of the system's time-dependent dipole moment. This dipole moment interferes coherently with the XUV excitation pulse and leads to the absorption spectrum, which also encodes the laser-induced changes as illustrated in figure 1(a) and further explained in [28]. This interferometric understanding of transient absorption intuitively explains the sensitivity to laser-induced phase and amplitude modifications of resonances [29–31].

Since the XUV pulse can ionize the system as well, the dipole moment between the continuum and the ground state is also expected to give rise to light-induced structures in the transient absorption spectra. These structures, too, are expected to be sensitive to light-induced phase shifts of the continuum states, which are dressed within the time-delayed strong laser pulse. We point out that this XUV-induced dipole response depends on the spatial wave function overlap between the excited states and the ground state. Thus, by using absorption spectroscopy one directly probes laser-induced dynamics when the ionized electron is still in close proximity of the residual ion, where the dynamics are expected to be most strongly influenced by the Coulomb potential. Modifications of the XUV absorption spectrum for a smooth continuum were addressed in [32] and around the ionization threshold in [25–27, 33] accompanied by a thorough discussion of laser-induced couplings between bound states.

In this work, we investigate the laser-field-modified dipole response of the continuum threshold of helium by means of XUV transient absorption spectroscopy in the presence of a near infrared (NIR) laser pulse; see figure 1. A recently developed *in situ* method for the recording of the XUV reference spectrum in transient absorption facilitates the observation of weak structures in the absorption spectrum at energies closely above the ionization threshold [34]. Comparing these structures with a model simulation we demonstrate direct sensitivity to laser-induced energy shifts of the ionized electron in the XUV photoabsorption spectrum. The measured results are further compared with a quantum-dynamical model simulation. Within this model, one can selectively switch on and off the presence of the continuum or the coupling between the continuum and the bound states. By doing so, we identify and isolate the signatures of the laser-driven response of the ionization threshold.

The spectra are recorded by an XUV beamline further discussed in [34]. In brief, attosecond pulses are created via high-order harmonic generation in xenon using an NIR laser pulse of sub-5 fs full-width-at-half-maximum (FWHM) pulse duration. A fraction of the co-propagating NIR pulse, with a peak intensity of about $10^{12}$ W cm$^{-2}$, and the XUV pulse are both focused with a variable time delay into a 3 mm long helium gas target with 50 mbar backing pressure.

The XUV transmission spectrum and the *in situ* XUV reference spectrum are recorded for different time delays between the NIR and XUV pulses by a grating-based spectrometer, figure 1(a). The photon flux of the main XUV beam is—without the helium target—about eight times higher than the photon flux of the corresponding reference beam. Considering this flux calibration factor $c$ and taking the intensity ratio of the transmission spectra $I_{\mathrm{Signal}}(\omega)$ and the reference spectra $I_{\mathrm{Ref}}(\omega)$ we calculate the XUV absorbance of helium in units of optical

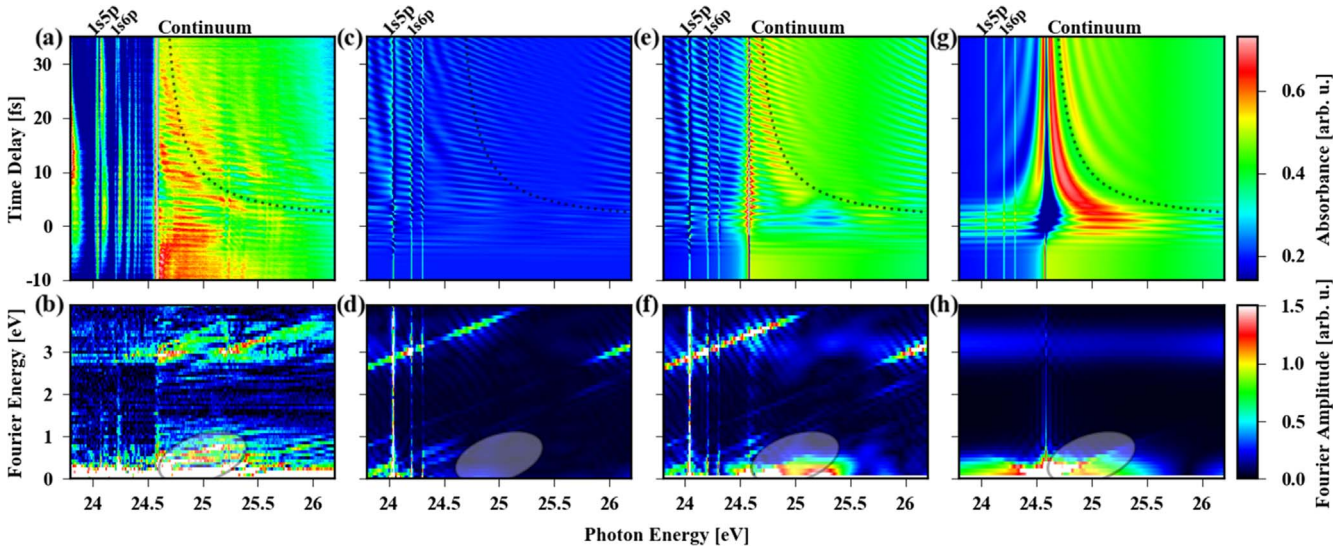


**Figure 2.** Measured and simulated attosecond transient absorption spectra of the first ionization threshold of helium. (a) Measurement for different time delays between the XUV excitation and the NIR coupling. Positive time delays mean that the NIR follows the XUV. For better visibility we increased the absorbance below threshold by 0.8 and the hyperbolic structure discussed in the main text is indicated by a black dotted line, likewise in (c), (e) and (g). (b) Fourier amplitude with respect to the time-delay axis in (a) with shaded area marking the region of interest. (c), (d) Simulation results, where only bound states are considered. The signal is multiplied by a factor of 10 for enhanced visibility. Well-known sharp Fourier features are reproduced. (e), (f) Absorption and Fourier spectra, where the continuum is included in the simulation. Broad Fourier features appear above the ionization threshold and low Fourier energy, resembling the measured data. (g), (h) Absorption and Fourier spectra, where the NIR acts only by introducing the laser-dressed canonical momentum $p \rightarrow p - A$ to the continuum state. The corresponding ponderomotive energy shifts lead directly to the hyperbolic structure (dotted line) at the ionization threshold, in agreement with the measurement.

density (OD) via the Lambert–Beer law:

$$\mathrm{OD}(\omega) = -\log_{10}\left(\frac{I_{\mathrm{Signal}}(\omega)}{c \cdot I_{\mathrm{Ref}}(\omega)}\right). \tag{1}$$

Figure 1(c) shows in blue solid line the measured static XUV photoabsorption spectrum without the NIR laser. The step-like increase of the absorbance above the ionization threshold at ∼24.58 eV is clearly observed. Figure 2(a) depicts the measured absorbance for different time delays between the XUV and NIR pulses. Various time-delay-dependent features are observed at energies below the first ionization threshold of helium. These light-induced structures around coupled resonances have been thoroughly studied and understood in previous works [24–27, 29].

Concerning XUV photon energies higher than the ionization threshold, we observe mainly two characteristic features. The first is a fast NIR-half-cycle oscillation, which appears across a broad spectral range both below and above the ionization threshold. To investigate this in more detail, we depict in figure 2(b) the amplitude of the Fourier transform with respect to the time-delay axis. The fast oscillation leads to diagonal Fourier peaks around 3.2 eV in Fourier energy, which corresponds to twice the NIR central photon energy of about 1.6 eV, thereby indicating a two-NIR-photon coupling process [26, 27, 29]. The second feature is a slow hyperbolic structure after the XUV-NIR temporal overlap, which converges to photon energies close to the continuum edge for increasing time delays (indicated by the dotted lines in figures 2(a), (c), (e) and (g)). This structure leads to a diagonal feature of the Fourier amplitude near zero Fourier energy (shaded area in figures 2(b), (d), (f) and (h)), which intersects the photon-energy axis to XUV energies of the Rydberg states and the continuum threshold. Similar structures were observed in photoelectron spectra and have been interpreted by the quantum beating of Rydberg states and the interference of direct and indirect ionization pathways [18].

In order to mechanistically understand the contribution of the ionization continuum on the features in the time-delay-dependent absorption spectrum, we apply a quantum-mechanical multi-level model to simulate numerically this absorption response in helium. It is calculated by the complex-valued time-dependent dipole moment $d(t, \tau)$ between the levels. With this dipole moment, we can generate the XUV photoabsorption cross section for every NIR-XUV time delay position $\tau$ via (see, e.g. [35])

$$\sigma(\omega, \tau) \propto \mathbb{Im}\left\{\frac{\tilde{d}(\omega, \tau)}{\tilde{E}(\omega)}\right\}, \tag{2}$$

where $\tilde{d}(\omega, \tau)$ is the Fourier transform of $d(t,\tau)$ and $\tilde{E}(\omega)$ is the complex-valued XUV excitation spectrum. This cross section is proportional to the XUV absorbance, which can be compared to the measured data taking into account the experimental spectrometer resolution of $\sim 10^{-2}$ eV.

In this coarse-grained model we numerically propagate the energy levels, which are represented by bound states, as well as discrete continuum states in the Schrödinger equation by a split-step algorithm, [36]. The entire state at a certain time $\Psi(t) = \sum_i \alpha_i(t)\phi_i + \sum_j \beta_j(t)\chi_j$ is then given by a superposition of bound ($\phi_i$) and continuum ($\chi_j$) states with their corresponding time-dependent complex-valued state

amplitudes $\alpha_i(t)$ and $\beta_i(t)$, respectively and the XUV and NIR pulses induce transitions and couplings among these states; see figure 1(b).

Initially, only the ground state is occupied and the weak XUV pulse perturbatively populates all *p*-symmetry excited states via dipole-allowed transitions. Our model includes the bound states with even and odd parities, the *s*-, *p*- and *d*-symmetries up to $1s4s$, $1s5p$ and $1s8d$, as well as the odd-parity continuum states $1sEp$. The sampling of the continuum states is set such that both the step-like increase of the absorption at the ionization threshold and the flat absorption spectrum for higher energies are reproduced; see figure 1(c). For this purpose, we use 200 spectrally overlapping discrete levels for the representation of the continuum.

The XUV pulse is modeled by a $\cos^2$ -shaped envelope in time with pulse duration of 150 attoseconds FWHM and centered at 24.5 eV photon energy, which leads to a sufficiently broad excitation spectrum with well-defined limits covering the XUV energy region of interest between 20 and 30 eV. The time-delayed NIR pulse has a Gaussian intensity profile, a duration of 5 fs FWHM, a central photon energy of 1.6 eV, and a peak intensity of $\sim 3.5 \times 10^{12}$ W cm$^{-2}$, as is the case in the experiment. Further details of the model simulation, together with a test of the dependency of the observed features on the model, can be found in the appendix.

To isolate structures of NIR-induced bound-bound transitions, we first consider only the bound states together with the NIR-induced dipole couplings among these states. Figure 2(c) depicts the simulated time-delay-dependent absorbance for this configuration and already qualitatively shows the experimentally observed structures, for instance, the half-NIR-cycle modulation around the energy of the ionization threshold leading to the diagonal Fourier feature at 3.2 eV Fourier energy; see figure 2(d). The origin of this feature at these photon energies is the all-optical interference between the direct XUV light and the delayed XUV-NIR transitions through the $1snp$ state, thereby creating a light-induced state. This is consistent with previous observations, and the presence of the continuum threshold is actually not necessary for its explanation [26, 27, 29]. However, almost no Fourier signal is present close to zero Fourier energy and at XUV photon energies above the ionization threshold, whereas the measured data show rich structures in this region.

By adding the continuum states to the state manifold of the simulation, additional features arise, which are shown in figures 2(e) and (f). First, the sharp absorption step at the ionization threshold of 24.58 eV is reproduced. Second, the hyperbolic structures above the ionization energy become more pronounced in the time-delay-dependent absorption spectrum. In agreement with the experimental observation, this leads to Fourier features pointing to the ionization threshold on the photon energy axis for small Fourier energies. This is illustrated by the shaded area in figure 2(f).

Exploiting the modularity of the multi-level model, we can obtain further insight into the origin of this hyperbolic structure in the continuum absorption spectrum. One can switch off the NIR-induced dipole couplings between the bound and continuum states, i.e. by artificially setting their dipole matrix elements to zero. By doing so, the NIR only induces an energy shift of the free electron's kinetic energy, expressed in atomic units by

$$E_n(t) = \frac{(p_n - A(t))^2}{2}. \tag{3}$$

Here $A(t) = -\int_{-\infty}^{t} E(t')dt'$ is the time-dependent vector potential of the NIR electric field $E(t)$, which adds a ponderomotive shift to the energy $E_n(t)$ of the continuum states with momentum $p_n$. The resulting time-delay-dependent absorption spectrum (see figures 2(g) and (h)) readily shows the hyperbolic structure at the continuum threshold, as observed in the measurement. Thus, the ponderomotive energy shift (or ac-Stark shift, if the dipole couplings between the bound and continuum states are considered) of the electron being energetically close to the ionization threshold is sufficient to qualitatively explain the characteristic time-dependent perturbed response of the continuum onset. It is interesting to note that at the NIR laser intensity used here, the ponderomotive energy amounts to only $\sim$0.2 eV, much smaller than the photon energy. This may typically not be considered as a strong field, but here we clearly identify strong-field-induced ponderomotive dressing effects, owing to the high sensitivity to small energy shifts within XUV transient absorption spectroscopy.

To summarize, we have observed laser-induced changes of the XUV transient absorption spectrum in the vicinity of the first ionization threshold of helium. By comparing our measurement with a multi-level model simulation, we were able to identify and explain the spectro-temporal structures in the optical density both below and above the ionization threshold. In particular, we link the hyperbolic structures at the ionization threshold to the NIR-induced energy shift of the photoelectron's kinetic energy in the vicinity of the atomic core. Furthermore, we found that the ionization threshold shows a similar—not *a priori* clear—behavior in the time-resolved absorption spectra, as is the case for bound-bound transitions. Thus, attosecond transient absorption spectroscopy is a powerful tool to study light–matter interaction or dynamics not only between bound states but can be extended to the continuum of states near an ionization threshold. Being able to extract field-driven dynamics near an ionization threshold even at moderate laser intensities is helpful especially for related attosecond transient absorption spectroscopy experiments in the condensed phase [37], where damage thresholds typically set an upper limit to the allowed laser intensity.

## Acknowledgments

We acknowledge funding from the European Research Council (ERC) (X-MuSiC-616783). The work of K B was supported by the United States National Science Foundation under grant No. PHY-1803844.

## Appendix

### *Details of the multi-level model simulation*

Each state $n$ in the multi-level model simulation has a certain decay constant $\Gamma_n$, energy position $E_n$ and dipole moments to the other states. The XUV photoabsorption calculated by equation (2) is dominated by the dipole moment between the ground state and the excited or continuum states. If the atom is ionized, i.e. the system is excited into continuum states, the liberated electron will leave the parent ion. Thus, the electronic wave function in the continuum and the ground-state wave function will lose the overlap over time, and hence the dipole moment between these states decreases. In order to account for this in our model, we introduce an effective decay for the continuum states. We set their decay constant to scale linearly with the momentum $p_n$ of continuum state $n$, which is given in atomic units by its energy and the ionization potential $I_p$:

$$\Gamma_n \propto p_n = \sqrt{2(E_n - I_p)}\,. \tag{A1}$$

By doing so, we obtain non-zero absorption linewidths for the continuum states in the absorption spectrum. Provided the energy difference between adjacent continuum states is less than $\sim 1/4$ of their decay constants, all continuum absorption lines will spectrally overlap and lead to the flat absorption spectrum shown by the orange dashed line in figure 1(c).

The energetically lowest continuum state is located at the ionization threshold of helium ($E_0 = 24.58\,\mathrm{eV}$). For the sampling of the energy positions of the other continuum states we assume that the electron is in a box potential. The energy of the continuum state $n$ is then given by: $E_n = \varepsilon\, n^2$, where we set $\varepsilon = 10^{-5}\,\mathrm{eV}$, which is three orders of magnitude smaller than the energy resolution of the measurement.

The values for the dipole moments between the bound states are taken from [38]. The dipole moments between bound and continuum states are approximated by hydrogenic atomic structure theory. Here, the continuum wave functions are Coulomb wave functions, which are the solutions of the Schrödinger equation of the hydrogen atom with positive energy [39, 40]. In the model, we use an effective charge $Z_{\mathrm{eff}} = 1.4$ for the core in the calculation of the ground-state wave function, which was tuned to find agreement of the overall shape of the simulated and measured continuum absorption spectrum shown in figure 1(c).

Note that the combination of the models for the decay constant, the energy sampling, and the estimation of the dipole moments by the hydrogen wave function together already leads to the shape of continuum absorption that is similar to the measured spectrum. Tests showed that slight changes of the free parameters, i.e. $\Gamma_0$, $\varepsilon$ and $Z_{\mathrm{eff}}$ do not change the key findings discussed above. Furthermore, the presence of the continua with $s$- or $d$-symmetry does not change the appearance of the hyperbolic structures.

### *Test of the validity of the approximate model for the continuum*

We validate the last two statements by another simulation of the absorption spectrum with a different model. In this approach, all energies and dipole matrix elements are consistently calculated from wave functions $\psi_n(r)$, which are the solutions of the Schrödinger equation with an approximate potential for an electron in the field of the $He^+$ ionic ground state. This local potential $V(r)$ is defined on a numerical grid by

$$V(r) = -\frac{1}{r} - \left(\frac{1}{r} + 1.3313\right)\cdot e^{-3.0634r}. \tag{A2}$$

For small radii, this potential approximates the Coulomb potential as seen by an electron close to the doubly charged helium core. For larger radii, the potential converges to a Coulomb potential of a singly charged core, i.e. a helium atom, which is screened by the other bound electron. At the limit of the grid the potential is infinite and thus represents a box potential. The states' energies are obtained by diagonalization of the total Hamiltonian. The kinetic energy used for the calculation of the decay constant is the difference between the total energy and the potential energy $E_{n,kin} = E_n - E_{n,pot}$ and the potential energy is the expectation value of the potential $E_{n,pot} = \int_0^a \psi_n^*(r) \times V(r) \times \psi_n(r)\, r^2 dr$, where $a$ is the grid size.

The two free parameters, namely the total grid size $a$ and the discretization step size $h$, determine the number of states within a given energy interval and the number of bound states in the system. The model reproduces the bound-state energies with an accuracy of 1% or better and presents a systematic way to account (approximately) for the high-lying Rydberg states and to discretize the continuum. Its advantage is the continuous change of the density of states energetically across the ionization threshold from Rydberg-like to an $n^2$ dependence in a box potential. Furthermore, all continuum states with the relevant symmetries, i.e. the $s$-, $p$- and $d$-symmetries, are included. With this model, we can therefore test whether the even-parity continua affect the absorption spectrum. Finally, the sensitivity of the results shown in this paper on the choice of $a = 800$ a.u. and $h = 0.1$ a.u., as well as the highest principal quantum number ($n = 200$) of the states included, was checked, and the results were found to be well converged.

The resulting time-dependent absorption spectra are shown in figure A1. We observe again the hyperbolic structure above the ionization threshold. This structure leads to the diagonal Fourier feature pointing to the ionization threshold indicated by the shaded area in figure A1(b). We conclude that the laser-induced hyperbolic structure is insensitive to the exact modeling of the continuum. Instead, it is a universal feature of the field-driven response of an ionization threshold.

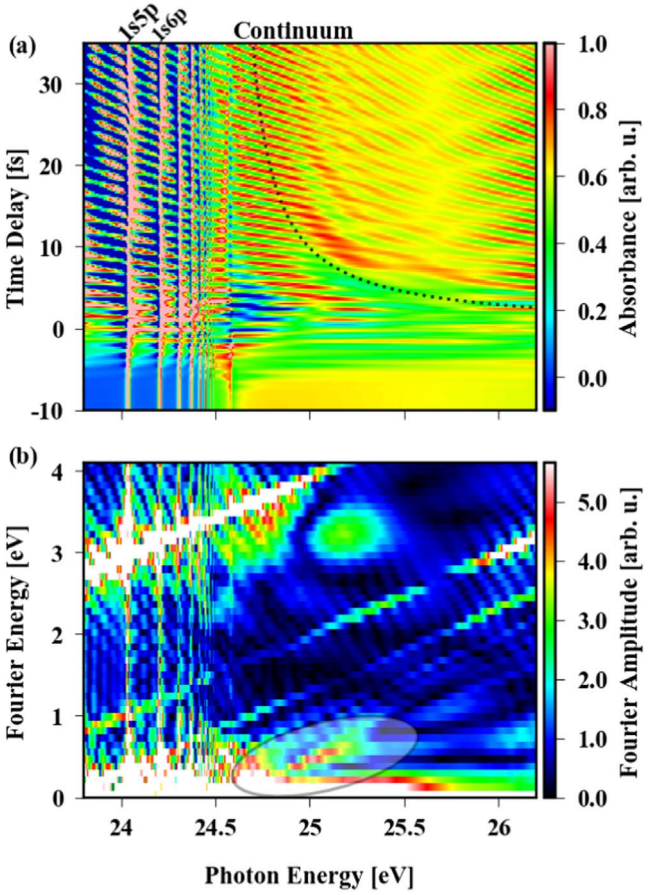


**Figure A1.** (a) Simulated absorption spectra of the first ionization threshold with the $He^+$ potential. Positive time delays mean that the NIR follows the XUV pulse. (b) Fourier amplitude with respect to the time-delay axis in (a) with shaded area marking the region of interest.

## ORCID iDs

Paul Birk https://orcid.org/0000-0002-1405-5155
Maximilian Hartmann https://orcid.org/0000-0002-6494-9368
Gergana D Borisova https://orcid.org/0000-0003-3558-3093
Tobias Heldt https://orcid.org/0000-0001-8156-3793
Klaus Bartschat https://orcid.org/0000-0001-6215-5014
Christian Ott https://orcid.org/0000-0003-4110-0916
Thomas Pfeifer https://orcid.org/0000-0002-5312-3747

## References

[1] Goulielmakis E *et al* 2010 Real-time observation of valence electron motion *Nature* **466** 739–43
[2] Wang H, Chini M, Chen S, Zhang C-H, He F, Cheng Y, Wu Y, Thumm U and Chang Z 2010 Attosecond time-resolved autoionization of argon *Phys. Rev. Lett.* **105** 143002
[3] Reduzzi M, Feng C, Chu W-C, Dubrouil A, Calegari F, Nisoli M, Frassetto F, Poletto L, Lin C-D and Sansone G 2013 Attosecond absorption spectroscopy in molecules *Conf. on Lasers and Electro-Optics (San Jose, CA)* (Washington, DC: OSA) QF2C.1
[4] Warrick E R, Cao W, Neumark D M and Leone S R 2016 Probing the dynamics of Rydberg and valence states of molecular nitrogen with attosecond transient absorption spectroscopy *J. Phys. Chem.* A **120** 3165–74
[5] Drescher M, Hentschel M, Kienberger R, Uiberacker M, Yakovlev V, Scrinzi A, Westerwalbesloh T, Kleineberg U, Heinzmann U and Krausz F 2002 Time-resolved atomic inner-shell spectroscopy *Nature* **419** 803–7
[6] Uiberacker M *et al* 2007 Attosecond real-time observation of electron tunnelling in atoms *Nature* **446** 627–32
[7] Cavalieri A L *et al* 2007 Attosecond spectroscopy in condensed matter *Nature* **449** 1029–32
[8] Itatani J, Quéré F, Yudin G L, Ivanov M Y, Krausz F and Corkum P B 2002 Attosecond streak camera *Phys. Rev. Lett.* **88** 173903
[9] Swoboda M, Fordell T, Klünder K, Dahlström J M, Miranda M, Buth C, Schafer K J, Mauritsson J, L'Huillier A and Gisselbrecht M 2010 Phase measurement of resonant two-photon ionization in helium *Phys. Rev. Lett.* **104** 103003
[10] Ranitovic P, Tong X M, Hogle C W, Zhou X, Liu Y, Toshima N, Murnane M M and Kapteyn H C 2011 Controlling the XUV transparency of helium using two-pathway quantum interference *Phys. Rev. Lett.* **106** 193008
[11] Shivaram N, Timmers H, Tong X-M and Sandhu A 2012 Attosecond-resolved evolution of a laser-dressed helium atom: interfering excitation paths and quantum phases *Phys. Rev. Lett.* **108** 193002
[12] Muller H G 2002 Reconstruction of attosecond harmonic beating by interference of two-photon transitions *Appl. Phys.* B **74** 17–21
[13] Schultze M *et al* 2010 Delay in photoemission *Science* **328** 1658–62
[14] Klünder K *et al* 2011 Probing single-photon ionization on the attosecond time scale *Phys. Rev. Lett.* **106** 143002
[15] Kheifets A S, Bray A W and Bray I 2016 Attosecond time delay in photoemission and electron scattering near threshold *Phys. Rev. Lett.* **117** 143202
[16] Blaga C I, Catoire F, Colosimo P, Paulus G G, Muller H G, Agostini P and DiMauro L F 2009 Strong-field photoionization revisited *Nat. Phys.* **5** 335–8
[17] Haessler S *et al* 2009 Phase-resolved attosecond near-threshold photoionization of molecular nitrogen *Phys. Rev.* A **80** 011404
[18] Mauritsson J *et al* 2010 Attosecond electron spectroscopy using a novel interferometric pump-probe technique *Phys. Rev. Lett.* **105** 053001
[19] Lucchini M, Ludwig A, Zimmermann T, Kasmi L, Herrmann J, Scrinzi A, Landsman A S, Gallmann L and Keller U 2015 Anisotropic emission in quantum-beat spectroscopy of helium excited states *Phys. Rev.* A **91** 063406
[20] Pazourek R, Reduzzi M, Carpeggiani P A, Sansone G, Gaarde M and Schafer K 2016 Ionization delays in few-cycle-pulse multiphoton quantum-beat spectroscopy in helium *Phys. Rev.* A **93** 023420
[21] Kazansky A K, Bozhevolnov A V, Sazhina I P and Kabachnik N M 2014 Attosecond near-threshold photoionization in a strong laser field *Phys. Rev.* A **90** 033409
[22] Azoury D, Krüger M, Orenstein G, Larsson H R, Bauch S, Bruner B D and Dudovich N 2017 Self-probing spectroscopy of XUV photo-ionization dynamics in atoms subjected to a strong-field environment *Nat. Commun.* **8** 1453
[23] Holler M, Schapper F, Gallmann L and Keller U 2011 Attosecond electron wave-packet interference observed by transient absorption *Phys. Rev. Lett.* **106** 123601

[24] Chen S, Bell M J, Beck A R, Mashiko H, Wu M, Pfeiffer A N, Gaarde M B, Neumark D M, Leone S R and Schafer K J 2012 Light-induced states in attosecond transient absorption spectra of laser-dressed helium *Phys. Rev.* A **86** 063408
[25] Chini M, Zhao B, Wang H, Cheng Y, Hu S X and Chang Z 2012 Subcycle ac stark shift of helium excited states probed with isolated attosecond pulses *Phys. Rev. Lett.* **109** 073601
[26] Chini M, Wang X, Cheng Y, Wu Y, Zhao D, Telnov D A, Chu S-I and Chang Z 2013 Sub-cycle oscillations in virtual states brought to light *Sci. Rep.* **3** 1105
[27] Chen S, Wu M, Gaarde M B and Schafer K J 2013 Quantum interference in attosecond transient absorption of laser-dressed helium atoms *Phys. Rev.* A **87** 033408
[28] Stooß V, Cavaletto S M, Donsa S, Blättermann A, Birk P, Keitel C H, Březinová I, Burgdörfer J, Ott C and Pfeifer T 2018 Real-time reconstruction of the strong-field-driven dipole response *Phys. Rev. Lett.* **121** 173005
[29] Blättermann A, Ott C, Kaldun A, Ding T and Pfeifer T 2014 Two-dimensional spectral interpretation of time-dependent absorption near laser-coupled resonances *J. Phys. B: At. Mol. Opt. Phys.* **47** 124008
[30] Ott C, Kaldun A, Raith P, Meyer K, Laux M, Evers J, Keitel C H, Greene C H and Pfeifer T 2013 Lorentz meets Fano in spectral line shapes: a universal phase and its laser control *Science* **340** 716–20
[31] Kaldun A *et al* 2016 Observing the ultrafast buildup of a Fano resonance in the time domain *Science* **354** 738–41
[32] Dahlström J M, Pabst S and Lindroth E 2017 Attosecond transient absorption of a bound wave packet coupled to a smooth continuum *J. Opt.* **19** 114004
[33] Lucchini M, Herrmann J, Ludwig A, Locher R, Sabbar M, Gallmann L and Keller U 2013 Role of electron wavepacket interference in the optical response of helium atoms *New J. Phys.* **15** 103010
[34] Stooß V, Hartmann M, Birk P, Borisova G D, Ding T, Blättermann A, Ott C and Pfeifer T 2019 XUV-beamline for attosecond transient absorption measurements featuring a broadband common beam-path time-delay unit and *in situ* reference spectrometer for high stability and sensitivity *Rev. Sci. Instrum.* **90** 053108
[35] Wu M, Chen S, Camp S, Schafer K J and Gaarde M B 2016 Theory of strong-field attosecond transient absorption *J. Phys. B: At. Mol. Opt. Phys.* **49** 062003
[36] Feit M, Fleck J and Steiger A 1982 Solution of the Schrödinger equation by a spectral method *J. Comput. Phys.* **47** 412–33
[37] Schultze M *et al* 2014 Attosecond band-gap dynamics in silicon *Science* **346** 1348–52
[38] Drake G 2006 High precision calculations for helium *Springer Handbook of Atomic, Molecular, and Optical Physics* (New York: Springer) pp 199–219
[39] Hill R 2006 Hydrogenic wave functions *Springer Handbook of Atomic, Molecular, and Optical Physics* (New York: Springer) pp 153–71
[40] Stobbe M 1930 Zur Quantenmechanik photoelektrischer Prozesse *Ann. Phys.* **399** 661–715